

Doppler imaging: the polar spot controversy

J.H.M.J. Bruls¹, S.K. Solanki², and M. Schüssler¹

¹ Kiepenheuer-Institut für Sonnenphysik, Schöneckstrasse 6, D-79104 Freiburg, Germany

² Institut für Astronomie, ETH-Zentrum, CH-8092 Zürich, Switzerland

Received 16 January 1998 / Accepted 28 April 1998

Abstract. Doppler imaging studies have revealed that most rapidly rotating cool stars have high-latitude spots, which in many cases cover the stellar poles. The spectroscopic signature of polar spots is a filling in of the cores of spectral lines, which become flat-bottomed and may show bumps. Although the existence of polar spots is corroborated by spectroscopic and photometric measurements, and although theoretical models predict polar spots, they remain controversial. Most notably, it has been proposed that the line core filling in might also be caused by chromospheric activity. We present a NLTE radiative transfer analysis of 14 of the most-used Doppler-imaging lines which demonstrates that chromospheric activity can produce filling in of the observed line profiles only in a few of these lines. Moreover, such filling in is in general not of the type observed in the spectra of active stars. We are able to produce a flat-bottomed line core by concentrating the chromospheric activity near the poles, but only for two of the strongest lines, Fe I 5497 Å and Fe I 6430 Å. In the observations, however, also the weaker lines have flat-bottomed cores. Therefore, it is unlikely that polar spots are an artifact due to misinterpretation of the spectral signature of chromospheric activity. Nevertheless, we cannot exclude that chromospheric activity provides part of the filling in of the cores of some stronger lines; we present a diagnostic that may help to separate the contributions of chromospheric activity and spots.

Key words: line: profiles – stars: activity – stars: chromospheres – stars: imaging – stars: late-type – starspots

1. Introduction

Doppler imaging has become an important and powerful tool for investigating the distribution and evolution of long-lived stellar surface features, viz. starspots. It exploits the fact that, in the spectrum of a rapidly-rotating star, there is a correspondence between wavelength position in a spectral line and spatial position on the stellar disk. Due to this correspondence, a feature that traverses the stellar disk can produce a bump or a dip that moves across the the observed line profile. A brief schematic description of the technique can be found in Vogt & Penrod (1983), and

an in-depth analysis of the performance and limitations of the inversion routines that are being used to derive the stellar surface structures from a series of spectra was performed by, e.g., Vogt et al. (1987), Rice et al. (1989), Strassmeier et al. (1991), and Unruh & Collier-Cameron (1995).

The ‘spatial resolving power’ of this surface imaging technique depends on the ratio of the rotational broadening of spectral lines and the intrinsic (thermal and turbulent) line width; it is only useful if this ratio is larger than about 2. This sets a lower limit to the required rotational velocity; the stars that satisfy this criterion are fast rotators, which therefore have high activity levels. Rotation conserves the line equivalent width, so that with increasing rotation rate the spectral lines become shallower; therefore noise imposes an upper limit to the rotational velocity range. In practice, stars with rotation velocities in the range of 20 to 100 km/s are suitable candidates for Doppler imaging.

Many of the stars imaged with this technique have line profiles with a flat-bottomed core (e.g., Strassmeier 1990), i.e. the core is noticeably filled in with respect to some reference profile. Fig. 1 shows an example of the typical line profiles observed over a complete rotation of an active star, in this case HD 199 178. This filling in of the observed line core is nearly time-independent, and it is interpreted as due to large, stable and long-lived starspots at high latitudes, commonly called polar spots, features not observed on the Sun.

Even though a theoretical explanation for the existence of high-latitude spots has been given (Schüssler & Solanki 1992, Schüssler et al. 1996), and notwithstanding the host of spectroscopic and photometric evidence for their existence (e.g., Strassmeier 1990, Donati et al. 1992, Hatzes et al. 1996), they have been subject to controversy ever since they were proposed. In particular, it has been speculated (Byrne 1992, Strassmeier et al. 1993, Byrne 1996) that the filling in of the spectral line cores – the most direct evidence for polar spots – could also be due to chromospheric activity.

The identification of starspots relies on the correctness of the reference line profiles of the immaculate star, most notably their equivalent width and center-to-limb behavior. The exact shape of the profiles is in general less relevant: it is smeared out significantly due to the large rotation rate. Two types of reference profiles are in use: (1) computed line profiles (assuming

a ‘reasonable’ stellar model atmosphere) and (2) appropriately broadened observed line profiles of a slowly-rotating non-active star of the same spectral type. Both need to be treated with caution, since the high rotation rate may influence the star’s atmosphere, so that neither the atmosphere of a slowly-rotating star nor a theoretical model of such an atmosphere may represent the atmosphere of the more active star correctly (e.g., Byrne 1996). That this might happen is suggested by the fact that several lines that are considered photospheric in non-active cool stars show cores filled in by chromospheric emission in more active stars (for line core filling-in see Basri et al. 1989). Similarly, enhanced chromospheric emission and temperatures are seen in solar plagues.

In this paper we investigate the sensitivity of the profiles of some widely-used Ca I and Fe I Doppler imaging lines to chromospheric activity using schematic models of stellar chromospheres that are derived from semi-empirical models of solar active regions. When chromospheres come into play, the assumption of local thermodynamic equilibrium (LTE) may no longer hold for all lines. Nevertheless, all theoretical line profiles used in Doppler-imaging analyses are computed under the simplifying assumption of LTE. Therefore, we additionally make a comparison between the LTE profiles and the proper non-LTE profiles of these lines.

From a radiative transfer point of view, one of the most compelling arguments against chromospheric activity being the cause of the flat-bottomed line profiles lies in the fact that it occurs almost independently of the line strength. This means that whatever is causing the filling in of the line cores, it must be something that works over a significant height range in the atmosphere. Admittedly, the lines in Table 1 do not cover the entire range of line strengths; more ‘exotic’ lines, such as the Na I D doublet, the Mg I b triplet and even H α , have been proposed or used for Doppler imaging, but those lines a priori require the effects of a chromosphere to be included in the analysis. Unruh & Collier-Cameron (1997) showed that stellar surface structures obtained from Doppler imaging with the Na I D₁ line have less pronounced high-latitude structures and give more consistent light curves of AB Doradus than photospheric lines. This conclusion, however, is based on LTE line profiles which for such strong lines exaggerate the effect of a chromosphere and seem to partially cancel the spot signature. This suggests that a consistent non-LTE treatment of chromospheric emission effects is really needed for stronger lines. Even the weakest Doppler-imaging lines in our sample point in the direction of polar spots, and it is more challenging to explain how in those lines chromospheric activity could produce features that mimic a polar spot.

2. The model atoms

Table 1 lists the lines that we studied. In order to accurately describe their formation properties, we need rather extended model atoms of neutral calcium and neutral iron.

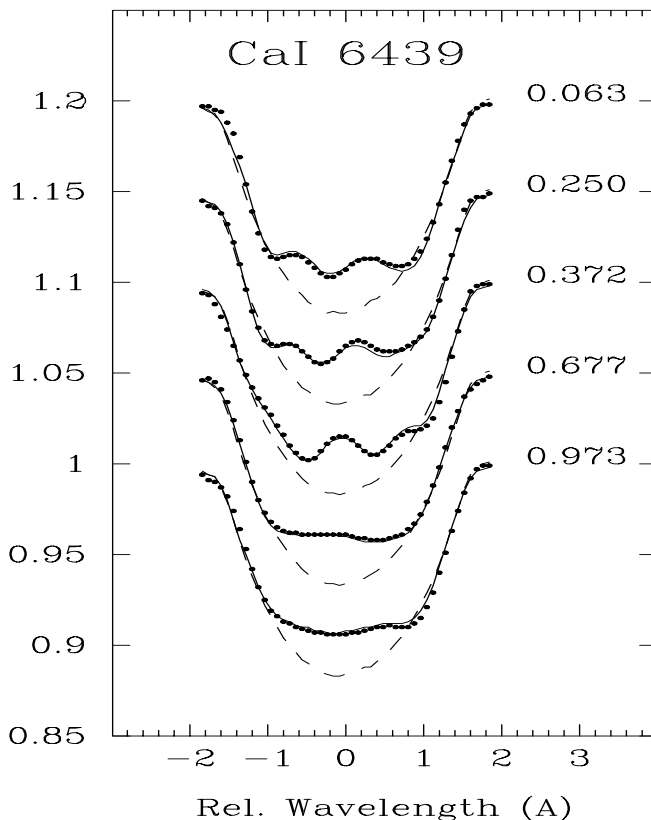


Fig. 1. Typical line profiles observed throughout a rotation cycle of HD 199 178. All profiles have been normalized to the neighboring continuum flux and the successively earlier phases have been incrementally offset by 0.05 for clarity. The respective phases are indicated to the right of the line profiles; the dots represent the observations, and the dashed curves the theoretical line profile without spots. A fit including starspots is denoted by the solid curves (figure kindly provided by K. G. Strassmeier)

2.1. The Fe I model atom

Reasonably accurate data are available for energy levels (Sugar & Corliss 1985; National Institute of Standards and Technology (NIST) atomic data compilation, available online as part of catalog VI/74 at NASA’s Astronomical Data Center¹, ADC, and mirrored at the Centre de Données astronomiques de Strasbourg², CDS), and transition probabilities (Fuhr et al. 1988; NIST data compilation, available online as part of catalog VI/72 at NASA-ADC and CDS) of neutral iron. That enabled us to construct a model atom that, apart from including all the Fe I lines in Table 1, provides some confidence that all levels and transitions that are important in setting the statistical equilibrium of iron are represented. In addition to a number of terms of singly-ionized iron, the dominant ionization stage throughout the photosphere and lower chromosphere, we selected all known triplet and quintet terms of neutral iron, and represent each by its most important sublevel, i.e. the level with the largest statistical weight. The multiplets connecting the se-

¹ <http://adc.gsfc.nasa.gov/adc.html>

² <http://cdsweb.u-strasbg.fr>

Table 1. The set of Doppler-imaging lines. In addition to the excitation energy, E , and the oscillator strength, $\log(gf)$, we list the location where the line center optical depth, τ_{ν_0} , reaches unity in the quiet Sun model FAL-C, both in terms of the standard optical depth τ at 5000 Å and in terms of geometrical height above $\tau = 1$

Wavelength Air, [Å]	E [eV]	$\log(gf)$	Quiet Sun: $\tau_{\nu_0} = 1$ @	
			$\log(\tau)$	Height [km]
Ca I 6122.215	1.89	-0.20	-2.80	370
Ca I 6166.436	2.52	-1.26	-0.97	130
Ca I 6439.072	2.53	-0.05	-2.21	290
Ca I 6462.564	2.52	-0.10	-2.17	290
Ca I 6717.680	2.71	-0.39	-1.71	230
Fe I 5497.515	1.01	-2.75	-3.22	420
Fe I 6141.728	3.60	-2.31	-0.53	60
Fe I 6157.723	4.08	-1.28	-1.17	150
Fe I 6165.358	4.14	-1.63	-0.69	90
Fe I 6173.338	2.22	-2.98	-1.45	190
Fe I 6180.200	2.73	-2.80	-1.01	130
Fe I 6411.644	3.65	-0.49	-2.51	330
Fe I 6430.841	2.18	-1.98	-2.72	360
Fe I 6546.236	2.76	-1.80	-2.21	290

lected terms are represented by the strongest line in each of them. All together the iron atom has 126 energy levels and 528 lines.

In addition to the NIST compilation of data, which are compiled from a multitude of sources, Thévenin (1989, 1990) provides a list of oscillator strengths from fitting the observed quiet Sun spectrum (Delbouille et al. 1973) in the wavelength range of 4000 to 8000 Å, albeit under the simplifying assumption of LTE. Most of the Fe I lines in this wavelength range, except perhaps the very strongest ones, are formed in the photosphere and Rutten & Kostik (1982) showed that due to the non-LTE masking phenomenon a simple LTE line strength analysis using an LTE solar model may well lead to the same results as a sophisticated non-LTE analysis using the best semi-empirical solar model available. It is for this reason that we selected Thévenin's oscillator strengths instead of the NIST values whenever possible. In particular, for all Doppler imaging lines themselves the gf -values have actually been taken from Thévenin (1989, 1990). The differences with the Fuhr et al. (1988) values are small, except in the case of the 6141.73 Å line for which Thévenin's oscillator strength is nearly an order of magnitude smaller (see Sect. 2.3).

Photoionization data for the lower levels were taken from Lites (1972), while for the other levels we assumed hydrogenic cross sections (Travis & Matsushima 1968). We computed collisional cross sections using the dipole approximation (Van Regemorter 1962), setting missing oscillator strengths to 0.1 for allowed transitions and 0.01 for forbidden transitions. Where possible, line broadening parameters were computed using measured a^2 values (Warner 1968) and lifetimes

(Corliss & Tech 1967, Kroll & Kock 1987); the Van der Waals broadening was computed using the approximation provided by Unsöld (1955) and enhanced by an excitation-energy dependent factor of up to 2.5, as suggested by the analysis by Simmons & Blackwell (1982).

2.2. The Ca I model atom

For neutral calcium the energy level data is available online in catalog VI/74 at NASA-ADC and CDS. Unfortunately, no oscillator strength data seem to be available there. For reasons of data handling convenience and data consistency, we obtained the energy level data indirectly, namely by extracting them together with the oscillator strengths from the list of Ca I lines on Kurucz's CD-ROM 23³. The only differences with the energy level data at NASA-ADC seem to be due to round-off errors. As in the case of the Fe I lines, whenever an oscillator strength could also be obtained from Thévenin (1989, 1990) that value was preferred. Unlike the neutral iron atom, the neutral calcium atom has a very regular structure and comparatively few energy levels, so that we need only 30 levels and 64 lines to accurately represent it.

Detailed photoionization cross sections are available from the Opacity Project (OP) database at CDS; we fitted a third order polynomial to the highly wavelength-dependent computed cross sections and resampled that at a convenient number of wavelengths. The OP data presented an unpleasant surprise: significant differences exist between the OP energy levels, which are computed self-consistently together with the photoionization cross sections and the oscillator strengths, and the actually measured values that are present in catalog VI/74 and on Kurucz's CD-ROM 23. That necessitated some wavelength shifts to match the actual wavelengths of the bound-free transitions. Collisional cross sections were obtained by means of the impact approximation (Seaton 1962, Bely & van Regemorter 1970).

2.3. Atomic data sanity check

With model atoms of the size used here, particularly when the data are not entirely available in computer-readable format, there is a significant danger that additional errors enter the model atoms.

By using the model atoms to compute non-LTE line profiles from the FAL-C (Fontenla et al. 1991) quiet Sun model atmosphere and comparing those with high-quality observed profiles (Brault & Neckel, unpublished, Kitt Peak FTS) one may hope to at least detect, explain and possibly fix the sources of the most severe deviations.

We found satisfactory but not perfect agreement (see Sect. 3 for more details) for all but the Fe I 6141 Å line. The computed profile of this line is much weaker than the observed line at that wavelength, which in reality is not a single line but rather a blend with a Ba II line that is stronger than the Fe I line. Without actually modeling the Ba II line, it is difficult to decide which oscil-

³ <http://cfa-www.harvard.edu/amp/data/kur23/sekur.html>

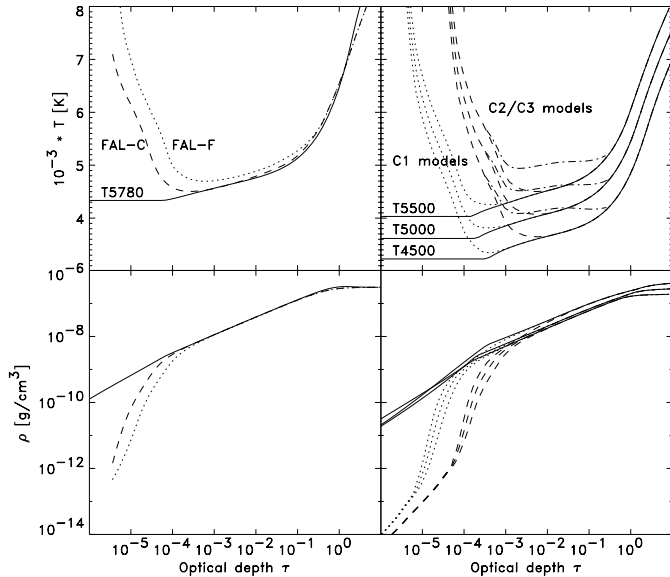


Fig. 2. The solar (left panels) and stellar (right panels) atmosphere models used. Top: temperature as a function of the standard continuum optical depth τ at 5000 Å; bottom: density as a function of τ

lator strength is better, but we decided to maintain Thévenin’s value. The presence of this blend strongly argues against the further use of this line for Doppler imaging studies.

Many uncertainties and inaccuracies undoubtedly remain. E.g., significant differences, up to about a factor of two, do exist between Thévenin’s oscillator strengths that we use here and the values of Kurucz’s CD-ROM 23 or of Fuhr et al. (1988), and there seems to be little or no correlation between these differences and the accuracy indication given by the latter authors. However, since it is not our intention to model observed line profiles in detail, but only to compare computed profiles with each other, they should play a minor role here. In the actual Doppler imaging inversions, such large errors in the line strengths may be disastrous (Strassmeier 1996).

3. The solar case

We used the Sun as the starting point of this analysis, basically in order to study the formation properties of the lines in our sample. In addition, we use the solar models to derive a recipe for adding a chromospheric temperature rise to a given stellar model atmosphere in order to model chromospheric activity in cooler stars.

The model atmospheres involved in this part of the analysis comprise two semi-empirical models, namely the quiet Sun model FAL-C and the solar average network model FAL-F by Fontenla et al. (1991), and the theoretical $T_{\text{eff}} = 5780$ K opacity distribution function (ODF) line blanketed radiative equilibrium (RE) model T5780 of Edvardsson et al. (1993). The temperature and density stratifications of the solar models are represented in the left panels of Fig. 2 as a function of the standard optical depth τ (at 5000 Å).

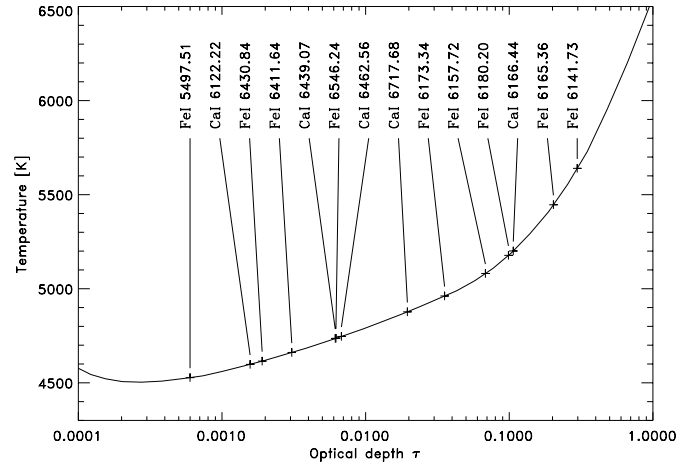


Fig. 3. ‘Formation heights’ of our lines in the FAL-C atmosphere, as indicated by the 5000 Å optical depth at which line center optical depth (τ_{ν_0}) unity is reached. The formation region of a line roughly covers the height range from its $\tau_{\nu_0} = 1$ location down to continuum optical depth $\tau = 1$. For all lines $\tau_{\nu_0} = 1$ lies below the temperature minimum, i.e. in the solar photosphere

3.1. The quiet Sun

Line profiles computed from the FAL-C model were compared with the profiles observed by Brault & Neckel to verify that the atomic data, in particular the oscillator strengths of the lines, are not too far off (Sect. 2.3). Exact line fits have not been attempted, since our comparison of theoretical profiles from atmospheres with and without chromospheric activity is not sensitive to such deviations. We have chosen to use the FAL-C model for these computations, instead of the T5780 model, because that model has been optimized as far as possible based on a broad range of observables. It should therefore lead to the (currently) best achievable theoretical non-LTE line profile fit; still, these cannot be exact since, among other things, a static plane parallel model atmosphere is not capable of producing the asymmetries that are commonly seen in observed line profiles and which are caused by convective flows.

The T5780 model produces slightly worse, but still acceptable, line profiles. The original T5780 model runs only up to $\tau \approx 5 \cdot 10^{-5}$, but it turned out to be necessary to extend that upwards. One can think of several ad hoc methods to establish such extension, the most obvious being linear extrapolation of T and $\log(\rho)$ vs. height. However, we opted against linear extrapolation, even though it would work for T5780, because we need to do the same for the stellar models (Sect. 4.1); for those models this procedure would result in excessively low temperatures. For consistency reasons we chose to extend all models with an isothermal layer in hydrostatic equilibrium.

In Fig. 3 we indicate the approximate formation heights of the line core, in the FAL-C atmosphere and at disk center, of all our lines. Since the lines are close in wavelength – in part due to the criterion that the lines should be free of blends and flanked by a clean continuum on both sides – it suffices to indicate the line center optical depth $\tau_{\nu_0} = 1$ locations. The formation

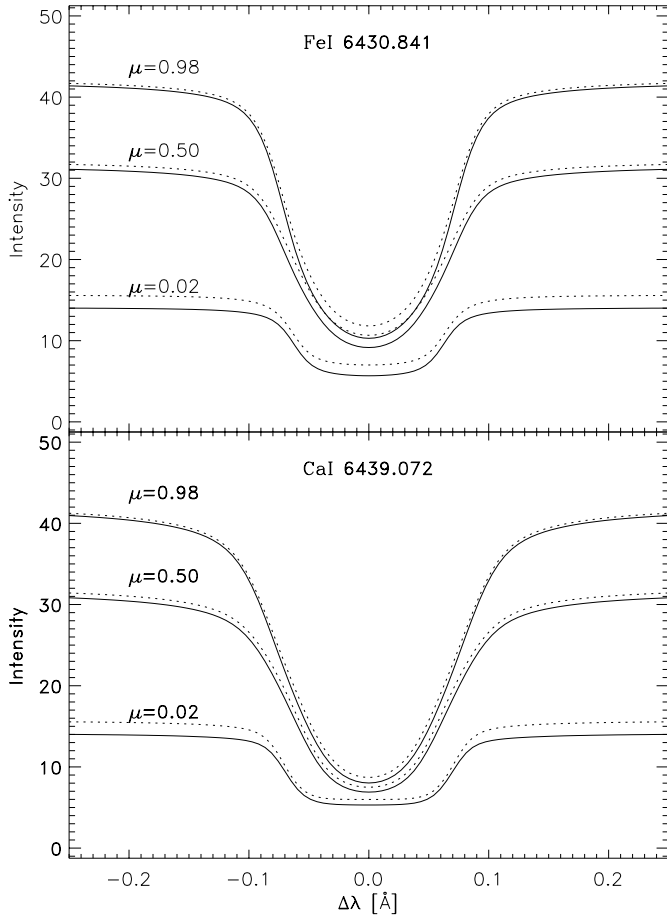


Fig. 4. Line profiles of Fe I 6430 Å and Ca I 6439 Å at three positions on the solar disk: $\mu = 0.98, 0.50$ and 0.02 . Solid curves are for the quiet Sun model FAL-C and dotted curves are for network model FAL-F. Intensities are in units of 10^{-6} erg/s/cm²/sr/Hz. The influence of chromospheric activity is largest for the Fe I line and even there it is negligibly small

height of the line wings approaches that of the neighboring continuum, whose formation differs only marginally from that of the continuum at 5000 Å. The formation range of each line approximately extends from its $\tau_{\nu_0} = 1$ location down to about standard continuum optical depth $\tau = 1$. Comparing with Fig. 2 it is immediately clear that all the lines in our sample are formed in the solar photosphere. Only a chromospheric temperature rise that is located considerably deeper in the atmosphere than in the average quiet Sun could influence their profiles.

3.2. Solar activity: influence on line profiles

As an example of the extremely small influence of chromospheric activity on our set of lines, we take a closer look at two of the most used lines in our sample: Fe I 6430 Å and Ca I 6439 Å, which are both reasonably strong lines. We use the FAL-F model to represent the chromospheric active atmosphere, since that has been optimized on the basis of observations. The resulting

profiles need to be compared with the quiet Sun (i.e. FAL-C) profiles to determine the influence of activity.

Fig. 4 compares the profiles of both lines for the FAL-C and FAL-F model atmospheres at three positions on the solar disk: $\mu = 0.98$ (disk center), $\mu = 0.50$, and $\mu = 0.02$ (limb). Here μ is the cosine of the heliocentric angle. This shows that on the Sun the effect of activity is very minor; the differences between the FAL-F line profiles and the quiet Sun profiles are so small that the change of the average solar line profile would not be observable in these spectral lines, even if as much as 10 percent of the surface were covered with activity.

4. The stellar case

Being neutral metal lines, the strength of the lines in our sample increases with decreasing temperature, so that it is expected that their sensitivity to activity may drastically rise for cooler stars. Using schematic chromosphere models in combination with radiative equilibrium photosphere models for such stars, we will show how activity influences the profiles of the Doppler imaging lines for cool stars.

4.1. The atmospheric models

In this section we use three atmospheric models of inactive stars, T5500, T5000 and T4500 (Fig. 2, right panels), which are opacity distribution function line blanketed radiative equilibrium models similar to T5780 with $T_{\text{eff}} = 5500, 5000$ and 4500 K, respectively, and with $\log(g) = 3.8$ (Edvardsson et al. 1993). Each of these models is extended outwards with an isothermal layer in hydrostatic equilibrium to allow some of the stronger lines to become optically thin below the upper boundary. Stellar activity is modeled by adding a schematic chromospheric temperature rise to such a model and recomputing the hydrostatic equilibrium; secondary effects, such as changes of the electron density induced by the temperature increase, are expected to be small and are therefore ignored. In a consistent model atmosphere, the electron density would rise as a consequence of increasing the temperature at chromospheric heights; the additional electrons have to come from ionization of the neutral metals, leading to lower neutral metal densities, deeper neutral metal line formation and reduced neutral metal line strengths. The lines that we compute from the present set of models will therefore be formed a bit too high in the atmosphere and accordingly the influence of chromospheric activity is overestimated.

The chromospheric temperature rise is derived from the available solar models in different ways. A first set of chromospheric temperature enhancements ΔT is obtained by subtracting the temperatures of the FAL-F and T5780 models, after a small offset to match the temperatures of both models in the mid and upper photosphere. That results in a temperature increment ΔT as a function of optical depth τ , which is non-zero only at $\tau < 10^{-3}$. These ΔT are added to the temperatures of the inactive atmospheric models to obtain the ‘activity models’ marked C1 (dotted curves in Fig. 2). The onset of the chromospheric temperature rise of the C1 models lies roughly at the

same optical depth as that of the chromospheric models derived by Mauas et al. (1997) for two dwarf M stars with very low ('basal') levels of chromospheric activity. This is what one may expect, given that our temperature increments are derived from models of the Sun, which is rather inactive as well.

We also constructed a more extreme set of activity models by shifting the temperature increment downward by one decade in optical depth, thereby simulating a very early chromospheric temperature rise. That leads to the activity models designated C2 (dashed curves in Fig. 2). The chromospheric parts of these models are similar to the models of solar magnetic flux tubes (Bruls & Solanki 1993, Briand & Solanki 1995) scaled to the appropriate effective temperature. Since small flux tubes represent by far the most extreme chromospheric temperature rise on the Sun we expect the C2 models to be rough estimates of the strongest possible chromospheres for the case when almost the whole star is covered with field, if the heating in magnetic elements is roughly independent of T_{eff} .

The chromospheres of the C2 models, however, are not nearly as strong as the *flare* models of AD Leo derived by Mauas & Falchi (1996). For that star the observed flare-induced continuum emission enhancement called for temperature increments with respect to the quiescent state model of AD Leo (Mauas & Falchi 1994) down to the optically thick regime of the photosphere, so that the temperature minimum actually ends up at $\tau > 10$. It is hard to imagine that a large fraction of the stellar surface could be covered by such extremely active regions for a large fraction of the time.

One might nevertheless argue that these two sets of schematic activity models do not represent the real world accurately enough. For example, one can think of a stellar analogue to the temperature difference between T5780 and FAL-F that we eliminated by means of a small offset before subtracting their temperatures in order to establish a model for the chromospheric temperature rise. Allowing also for such photospheric temperature enhancements would result in offsets in the line source functions with respect to our C1/C2 values that are expected to be small compared with the effects introduced by the chromospheric temperature enhancement. Nevertheless, since this enhancement could produce line profile changes for *all* lines, not just the ones that are formed high enough to notice the chromospheric temperature rise, we considered also a third class of model atmospheres, which we denote by C3 (dot-dashed curves in Fig. 2). These models have the same extreme temperature rise as the C2 models and in addition they have an enhanced photospheric temperature that reaches down to almost $\tau = 1$. The temperature enhancement was chosen such that $T(\tau)$ is almost constant throughout the photosphere. It is also much stronger than the photospheric temperature enhancement exhibited by FAL-F relative to FAL-C. In the following we systematically analyze the influence of a chromosphere using the C1 and C2 models and we use the C3 models only to illustrate that the conclusions deduced from the other sets of models apply equally to even stronger temperature enhancements.

4.2. Stellar activity: influence on line profiles

We start this section with an overview of the changes of the formation heights of our lines, both as a function of the effective temperature of the atmosphere and as a function of the type of chromosphere that is present. Fig. 5 presents the locations of line center optical depth unity for all lines across the set of model atmospheres. This figure is the stellar analogue to Fig. 3. We introduce three categories of lines, roughly, on the basis of their formation heights, although the allocation of some of the lines to a particular group may vary somewhat with the effective temperature of the atmosphere. The members of the first group, Fe I 5497, 6411, 6430, 6546 Å and Ca I 6122 Å, are formed rather high in the atmosphere and accordingly may exhibit a strong response to chromospheric activity. The second group, consisting of Fe I 6173 Å and Ca I 6439 and 6462 Å, is formed in the upper photosphere, and only weak to moderate response to chromospheric activity may be expected. The remaining six lines are formed so deep in the photosphere that they should be unaffected by chromospheric activity.

If LTE were a valid assumption, it would be easy to pick out the lines with the largest chromospheric influence in their profiles on the basis of the formation heights alone. Unfortunately, due to non-LTE effects, in particular scattering in the stronger lines, the true response to chromospheric activity of these lines is often smaller than formation heights suggest. Therefore, we also need to look at the behavior of the line source function when a chromospheric temperature rise is applied: most non-LTE line source functions do not follow the chromospheric temperature rise at all or only to a very limited extent. In addition, the source functions are in general only weakly height-dependent in those layers, so that changes in line optical depths due to the addition of a chromospheric temperature rise are not reflected strongly in the line profiles. The line shape is therefore largely preserved for most lines even though they become optically thin at chromospheric heights. It follows that only a few lines are really sensitive to what happens in the upper atmosphere: Fe I 5497, 6430 and 6546 Å show the strongest reactions to chromospheric activity, whereas Fe I 6173, 6411 Å and Ca I 6122, 6439, and 6462 Å are weakly sensitive. In all cases, the sensitivity decreases significantly with increasing effective temperature T_{eff} of the star.

For a look at the lines that do notice chromospheric activity, we select two representative lines, Fe I 6430 Å and Ca I 6439 Å. The former is the most chromosphere-sensitive line in our sample (together with Fe I 5497 Å), while the latter is only moderately sensitive, but is of particular interest since it is the most used Doppler imaging line. Fig. 6 shows the line source functions (left panels) and the corresponding line profiles (right panels) of Fe I 6430 Å, resulting from the inactive stellar atmosphere models (solid curves) and compares them with the line profiles resulting from the C1 (dotted curves) and C2 (dashed curves) activity models. Such line profiles are shown at three positions on the stellar disk (cf. Fig. 4). The line source functions (left panel) and the corresponding line profiles (right panel) of Ca I 6439 Å are plotted in Fig. 7, but only for the coolest stellar model; at

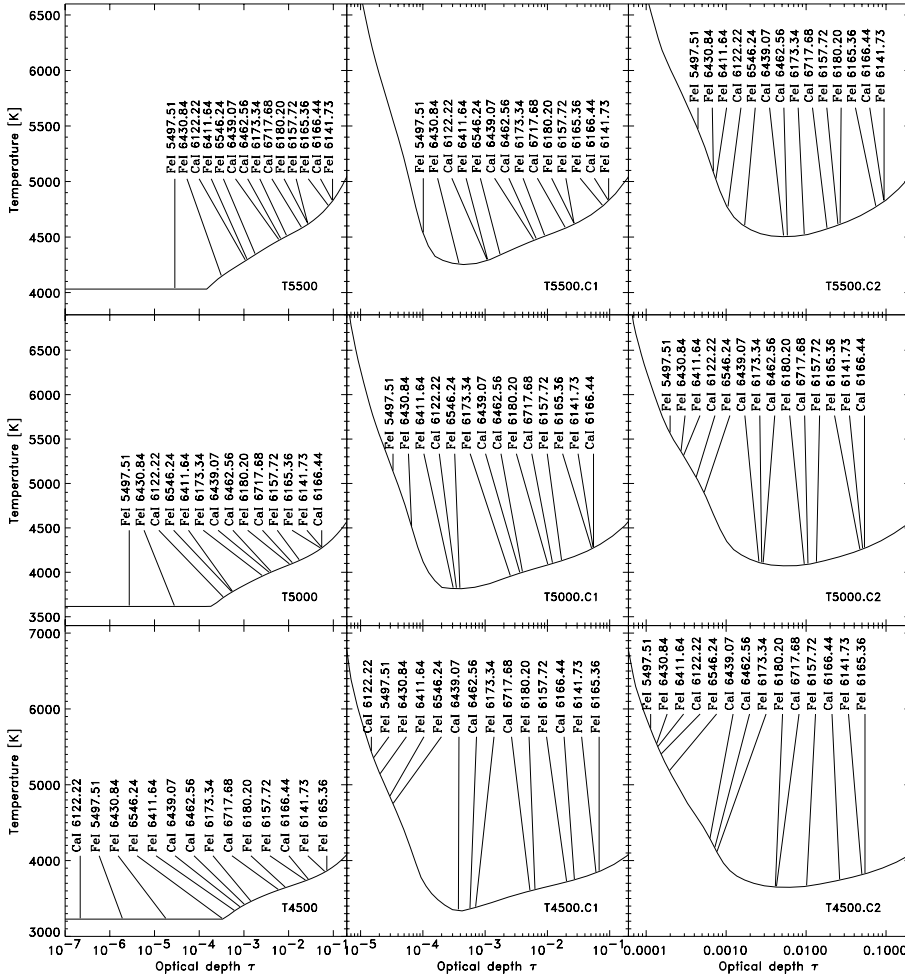


Fig. 5. Formation heights of our lines across a set of stellar atmospheres. Top to bottom: decreasing T_{eff} ; left-to-right: increasing strength of the chromosphere (the names of the atmospheres are indicated at the bottom-right of each frame). As in Fig. 3, for each line we indicate the location of line center optical depth $\tau_{\nu_0} = 1$; the formation region of a line approximately extends from $\tau_{\nu_0} = 1$ down to continuum optical depth $\tau = 1$. Especially for the cooler atmospheres the formation region of several lines reaches (far) up into the active chromosphere

higher effective temperature the sensitivity to activity is even less than at 4500 K, and it is clear that that is insufficient to be of any significance for the rotation-broadened disk-averaged line profile, no matter how high the surface coverage fraction of the active regions is. Only those line profiles of the Ca I line that originate from the very limb of the stellar disk show some response to activity, and that is just the location that would least contribute to any ‘polar spot’ artifact (see below). For the moment, we therefore continue with Fe I 6430 Å only. This line shows a very pronounced chromospheric emission feature at all positions of the stellar disk, including at disk center ($\mu = 1$).

4.3. Disk-integrated line profiles

The center-to-limb variation of the emission plays a vital role in determining the shape of the disk-integrated line profile. If, as in the case of Ca I 6439 Å, an emission core is present only near the limb of the star, we expect the disk-integrated profile to be narrower than in a star without a chromosphere. This is because the contribution of the limb is larger to the blue and red wings of the disk-integrated, rotationally-broadened profile than to its core. Hence we expect that for this and similar lines a chromosphere produces exactly the *opposite effect of a polar spot*.

In order to produce a flat-bottomed profile the emission must therefore either be stronger at the center of the stellar disk than at the limb, or the magnetic features possessing strong chromospheres must be inhomogeneously distributed on the stellar disk. None of our spectral lines shows a behavior consistent with the first of these possibilities. Even Fe I 6430 Å, which exhibits strong line core emission at disk center, is shown to emit even more strongly near the limb.

To obtain a better quantitative estimate of the effect described above we computed rotationally-broadened disk-averaged line profiles. They result from a careful integration of the non-LTE line profiles computed for each model atmosphere separately in plane-parallel fashion; the center-to-limb behavior of the computed line profiles is taken into account as well as their Doppler shifts due to the line-of-sight component of the rotation velocity. The stellar surface was represented by means of a mesh in polar coordinates, with a rotation-rate dependent grid spacing; typically 200 longitudes and 100 latitudes were needed to obtain sufficient accuracy in the integration.

Fig. 8 shows the disk-averaged line profile of Fe I 6430 from a star with $T_{\text{eff}} = 4500$ K that rotates (rigidly) at a rate of 30 km/s. The different curves are for varying amounts of surface coverage (filling factor) of the C2 activity model, assumed

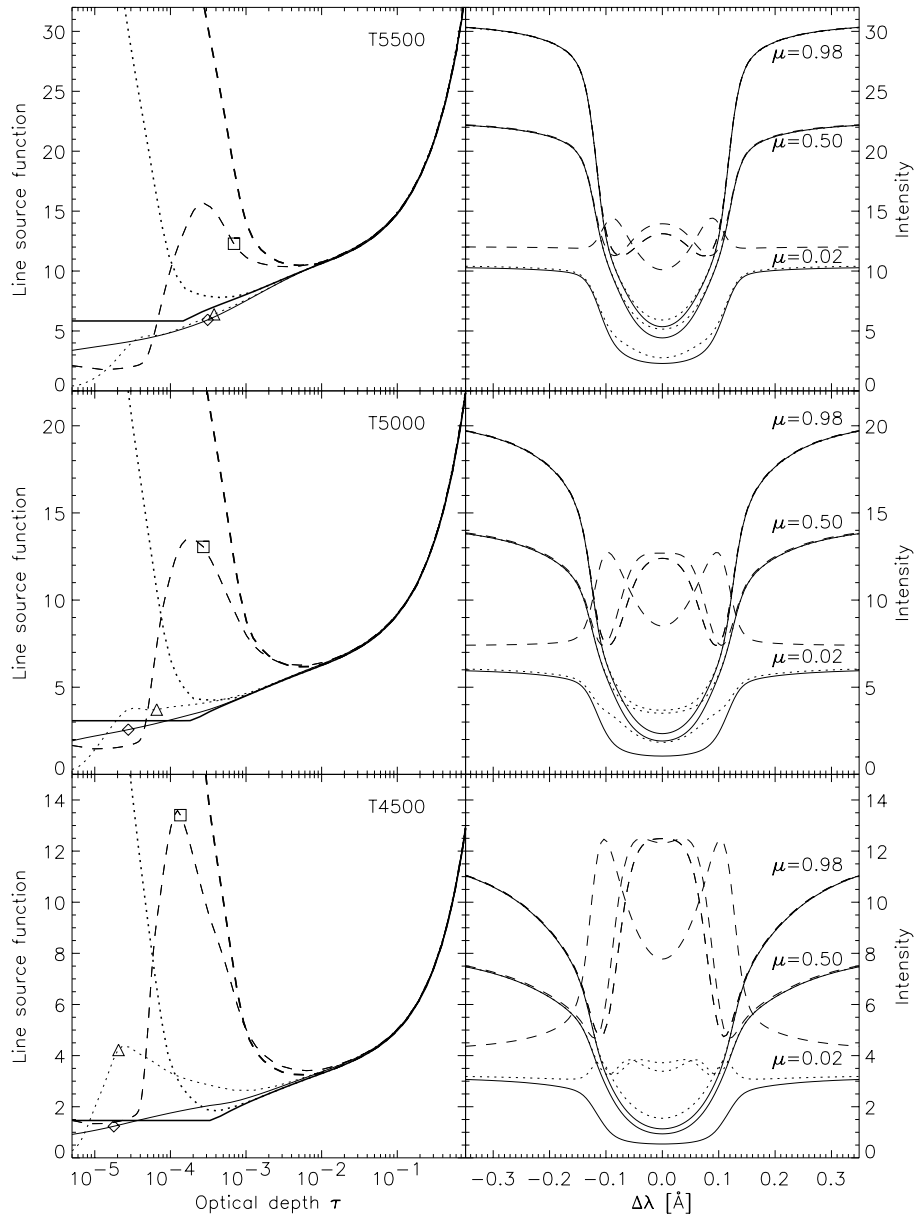


Fig. 6. Left panels: comparison of Fe 16430 \AA line source functions (thin curves) and Planck functions (thick curves). Solid curves are the inactive stellar models, dotted curves the C1 active models and dashed curves the C2 active models. Line center optical depth unity is indicated by diamonds (inactive models), triangles (C1 models) and squares (C2 models). Right panels: comparison of corresponding line profiles, for three positions on the stellar disk, $\mu = 0.98, 0.50$ and 0.02 . The same line styles apply as in the left panels. Top to bottom: $T_{\text{eff}} = 5500, 5000$ and 4500 K. Intensities, source functions and Planck functions are in units of 10^{-6} erg/s/cm²/sr/Hz. At all effective temperatures this line shows sensitive reaction to type C2 activity at all positions on the stellar disk, and some reaction, especially towards the limb, to C1 activity

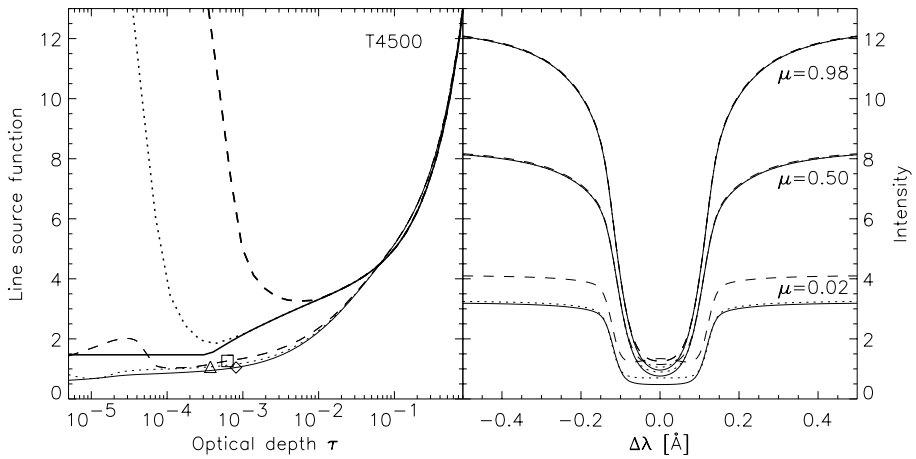


Fig. 7. The same as Fig. 6, but for Ca 16439 \AA and for $T_{\text{eff}} = 4500$ K only. This line is barely sensitive to even the strong C2 activity. Only near the extreme limb do some small profile changes occur. At higher effective temperatures the effect of activity is even smaller

to be uniformly distributed over the stellar surface. The line profiles shown are for inclination $i = 90^\circ$, i.e. the star's rotation axis is perpendicular to the line of sight. The line profiles for other values of i (not shown) have similar shapes, except that with decreasing i the line width decreases while the line depth increases (conserving the equivalent width). This combination of a low T_{eff} inactive stellar atmosphere with the C2 activity model produces the most prominent activity signatures in the line profiles. Obviously, the effect of including a certain surface coverage of the C2 activity model is not limited to the line core, but it changes the entire core and inner wing profile. As the filling factor is increased the dominance of the emission near the limb becomes increasingly evident until, for the case that the whole star is covered by a C2-like atmosphere, emission peaks occur in the inner wing of the profile. The decrease in the width of the profile in Fig. 8 with increasing chromospheric filling factor is also clearly visible. A homogeneous surface distribution of plage evidently cannot mimic polar spots.

Let us now turn to the second possible way of producing flat-bottomed profiles, namely by restricting the chromospheric temperature rise to certain locations on the stellar disk only. A way to limit the influence of the active regions to the core of the rotationally-broadened line profile at all rotational phases is to put such regions near the poles of the star. In this case the influence of the chromospheric emission will be restricted to the core of the disk-averaged profile, since the active regions now nearly coincide with the (projected) rotation axis, i.e. only small Doppler shifts apply to their line profiles. Since only quiet regions are present far from the rotation axis, the wings of the disk-averaged profiles remain unaffected by activity. The net effect of placing active regions at high latitudes will be an intensity enhancement in the line core; this effect is enhanced further by using an inclination, i , of the stellar rotation axis that differs (significantly) from 90° , so that the projected area of the polar active region, and hence its contribution to the disk-averaged line profile, increases. The top panel of Fig. 9 shows the line profiles of Fe I 6430 Å from the T4500 model with T4500.C2 activity within a certain area around the stellar poles. Indeed, the line core is filled in and the remainder of the line profile is unmodified. More importantly, for a certain size range of the polar active region, the core is virtually flat.

However, before dashing to the conclusion that therefore (polar) chromospheric activity may be put forward as an alternative for polar spots, let's look at the bottom part of Fig. 9, which shows the profiles of the Ca I 6439 Å line under the same circumstances. Those profiles totally lack a flat-bottomed line core.

In Fig. 10 we plot the same as in Fig. 9, but this time using the T4500.C3 activity model. Although the influence on the Ca I 6439 Å line core now appears stronger, the wings are enhanced by about the same amount and the profile shape is not markedly different. The result remains unchanged: Fe I 6430 Å exhibits a much more pronounced core filling than Ca I 6439 Å.

These results imply that simultaneous observations of both these lines could help to distinguish between the distribution of starspots and intense stellar plage regions. Whereas the pro-

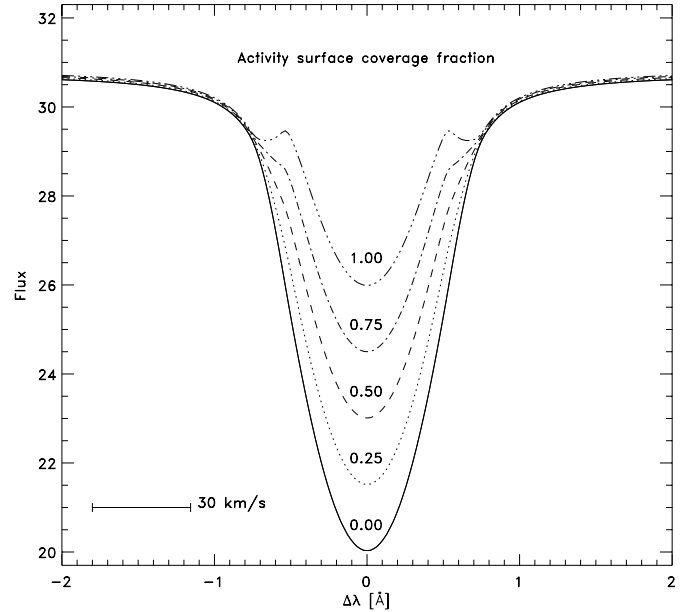


Fig. 8. Rotationally broadened line profiles of Fe I 6430 Å for a star with $T_{\text{eff}} = 4500$ K and a rotation rate of 30 km/s. Plotted are the line profiles for varying amounts of T4500.C2 activity, distributed uniformly over the stellar surface. Fluxes are in units of 10^{-6} erg/s/cm²/Hz. The resulting profiles do not all show the flat-bottomed core, which is taken as a signature of polar spots

file shape of Ca I 6439 Å only reveals the presence of starspots, Fe I 6430 Å is sensitive to both spots and plage. The main differences between the profile shapes of the two lines will therefore be due to the distribution of intense plage on the stellar surface.

5. Discussion

Flat-bottomed line cores are observed on rapidly-rotating cool stars and are commonly ascribed to spots near or at the stellar poles. The reality of polar spots has been a subject of debate, however. An alternative proposed in the literature is to have an inversion in the line core due to enhanced chromospheric emission. We have computed non-LTE line profiles for a set of widely-used Doppler imaging lines from cool stars with and without chromospheric activity, i.e. with and without a chromospheric temperature rise. We find that only very few of our lines are sensitive to even extreme amounts of chromospheric activity to an extent that would be visible in rotationally-broadened line profiles. In contrast, the observed profiles of *all* lines show flat-bottomed cores. In addition, the type of line profile changes induced by a uniform distribution of regions of chromospheric activity on the stellar surface is completely different from what is observed: almost the entire line profile is affected, not just the line core.

The way in which the line profile shape is affected can be influenced by restricting the chromospheric activity to certain places on the stellar surface (in particular to certain latitudes) instead of using a uniform distribution. We find that the line core can be filled in while the line wings are unaffected only if the

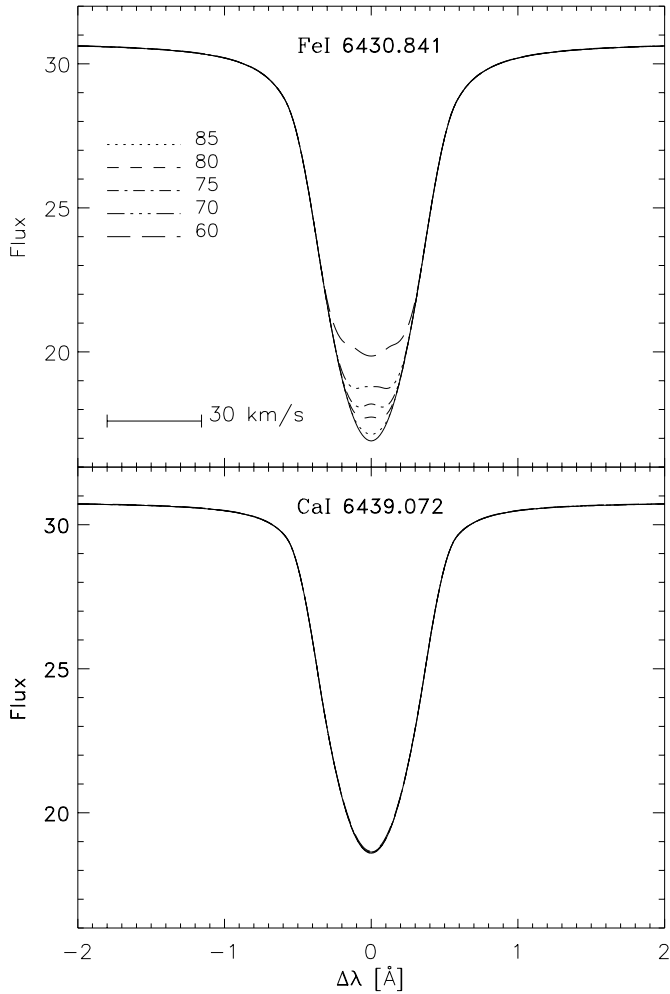


Fig. 9. Rotationally broadened line profiles of Fe I 6430 Å (top) and Ca I 6439 Å (bottom) for a star with $T_{\text{eff}} = 4500$ K and a rotation rate of 30 km/s with T4500.C2 active regions of varying extent placed at the poles. The various curves are labelled with the latitude (in degrees) above which the T4500.C2 activity model is applied and below which the inactive T4500 model is present. The star's rotation axis is inclined by 45° w.r.t. the line of sight. Fluxes are in units of 10^{-6} erg/s/cm²/Hz. The stronger Fe I line now has a flat-bottomed core, whereas the Ca I line is virtually unaffected by a chromospheric enhancement near the poles. Its behavior is typical of what happens to all weaker lines

chromospheric activity is located near the poles of the star. Our analysis nevertheless suggests that the observed flat-bottomed profiles are to a large part due to spots rather than plages. Line core filling such as that shown in Figs. 9 and 10 occurs for very few lines only, since most spectral lines are simply not sensitive enough to chromospheric or even photospheric temperature enhancements. We also propose a diagnostic, based on line profile observations of Fe I 6430 Å and Ca I 6439 Å, with which a separation of the plage and spot signals may be attempted.

One might speculate about other causes for the filling in of the line profiles. Unless one resorts to an inhomogeneous distribution of features (active regions, as explored above, or spots, obviously) with properties different from the average stel-

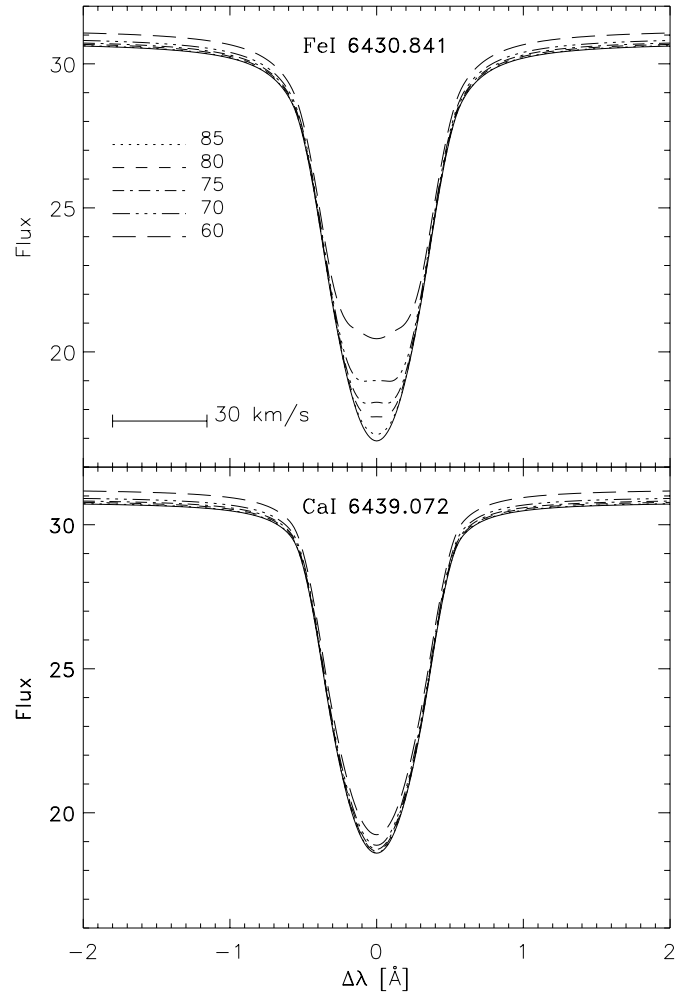


Fig. 10. The same as Fig. 9, but for T4500.C3 active regions.

lar atmosphere, essentially what one should look for are either uniformly-distributed atmospheric inhomogeneities or radiative transfer processes that preferentially enhance the intensity only near disk center⁴. We see two ways to obtain such an enhancement:

- A spatially constrained line source function enhancement, e.g. from some local heating process. It is difficult to model such structure, and, unless these hot blobs occur over a fairly large height range, they cannot explain why line center enhancements occur in stronger as well as weaker lines. But, if they do occur over a large height range, some lines will also show their effect near the limb, which inevitably leads to line cores that are no longer flat (Fig. 8).
- The current line profiles have been computed under the assumption that complete redistribution (CRD) is valid. In the cooler models the line formation occurs in higher layers and it may well be that partial frequency redistribution (PRD) may have to be applied to obtain correct line profiles. PRD profiles can indeed satisfy the requirement that the intensity

⁴ If rotational broadening is not so large, then the enhancement also needs to be concentrated near the core of the line.

enhancement should preferentially be strongest near disk center. Even so, for the weaker lines, CRD should remain valid.

Neither of these provides a satisfactory explanation why the flux enhancement occurs both in strong and in weak lines, i.e. independently of the line formation heights.

6. Conclusion

Chromospheric activity cannot be the *main* cause of the flat-bottomed line cores that are observed on many active stars, and therefore cannot challenge their interpretation in terms of polar spots.

Even if polar or high-latitude plages were to be responsible for a part of the line core filling observed in rapid rotators, this would not change the main picture of the magnetic-field distribution on such stars. Since plages are a magnetic phenomenon just as much as spots are, the magnetic field underlying the thermodynamic changes of the atmosphere must be concentrated at high latitudes irrespective of whether plages or spots cause the observed filled-in line cores on rapid rotators.

Acknowledgements. We thank Dr. K. G. Strassmeier for providing a typical example of observed line profiles with a filled-in core (Fig. 1) and Dr. Y. C. Unruh for help with the line selection.

References

- Basri G., Wilcots E., Stout N., 1989, *PASP* 101, 528
 Bely O., van Regemorter H., 1970, *ARA&A* 8, 329
 Briand C., Solanki S. K., 1995, *A&A* 299, 596
 Bruls J. H. M. J., Solanki S. K., 1993, *A&A* 273, 293
 Byrne P. B., 1992, in P. B. Byrne, D. J. Mullan (eds.), *Surface Inhomogeneities on Late-Type Stars*, Springer-Verlag, p. 3
 Byrne P. B., 1996, in K. G. Strassmeier, J. L. Linsky (eds.), *Stellar surface structure*, Proceedings IAU Symposium 176 (Vienna), Kluwer, Dordrecht, p. 299
 Corliss C. H., Tech J. L., 1967, *J. of Research of the NBS* 71A, No. 6, 567
 Delbouille L., Neven L., Roland G., 1973, *Atlas photométrique du spectre solaire*, Institut d'Astrophysique, Université de Liège
 Donati J.-F., Semel M., Rees D. E., 1992, *A&A* 265, 669
 Edvardsson B., Andersen J., Gustafsson B. et al., 1993, *A&A* 275, 101
 Fontenla J. M., Avrett E. H., Loeser R., 1991, *ApJ* 377, 712
 Fuhr J. R., Martin G. A., Wiese W. L., 1988, *J. Phys. Chem. Ref. Data* 17, Suppl. 4
 Hatzes A. P., Vogt S. S., Ramseyer T. F., Misch A., 1996, *ApJ* 469, 808
 Kroll S., Kock M., 1987, *A&AS* 67, 225
 Lites B. W., 1972, *Observation and Analysis of the Solar Neutral Iron Spectrum*, NCAR Cooperative Thesis No. 28, High Altitude Observatory, Boulder
 Mauas P. J., Falchi A., 1994, *A&A* 281, 129
 Mauas P. J., Falchi A., 1996, *A&A* 310, 245
 Mauas P. J. D., Falchi A., Pasquini L., Pallavicini R., 1997, *A&A* 236, 249
 Rice J. B., Wehlau W. H., Khokhlova V. I., 1989, *A&A* 208, 179
 Rutten R. J., Kostik R. I., 1982, *A&A* 115, 104
 Schüssler M., Solanki S. K., 1992, *A&A* 264, L13
 Schüssler M., Caligari P., Ferriz-Mas A., Solanki S. K., Stix M., 1996, *A&A* 314, 503
 Seaton M. J., 1962, *Proc. Phys. Soc. London* 79, 1105
 Simmons G. J., Blackwell D. E., 1982, *A&A* 112, 209
 Strassmeier K. G., 1990, *ApJ* 348, 682
 Strassmeier K. G., 1996, in K. G. Strassmeier, J. L. Linsky (eds.), *Stellar surface structure*, Proceedings IAU Symposium 176 (Vienna), Kluwer, Dordrecht, p. 289
 Strassmeier K. G., Rice J. B., Wehlau W. H. et al., 1993, *A&A* 268, 671
 Strassmeier K. G., Rice J. B., Wehlau W. H., Vogt S. S., Hatzes A. P., Tuominen I., Piskunov N. E., Hackman T., Poutanen M., 1991, *A&A* 247, 130
 Sugar J., Corliss C., 1985, *J. Phys. Chem. Ref. Data* 14, Supplement 2
 Thévenin F., 1989, *A&AS* 77, 137
 Thévenin F., 1990, *A&AS* 82, 179
 Travis L. D., Matsushima S., 1968, *ApJ* 154, 689
 Unruh Y. C., Collier-Cameron A., 1995, *MNRAS* 273, 1
 Unruh Y. C., Collier-Cameron A., 1997, *MNRAS* 290, L37
 Unsöld A., 1955, *Physik der Sternatmosphären*, 2nd edition, Springer, Berlin
 Van Regemorter H., 1962, *ApJ* 136, 906
 Vogt S. S., Penrod G. D., 1983, *PASP* 95, 565
 Vogt S. S., Penrod G. D., Hatzes A. P., 1987, *ApJ* 321, 496
 Warner B., 1968, *Zs. f. Ap.* 69, 161